The association of microbial activity with Fe, S and trace element distribution in sediment cores within a natural wetland polluted by acid mine drainage

DOI:
10.1016/j.chemosphere.2019.05.157

Document Version
Accepted author manuscript

The association of microbial activity with Fe, S and trace element distribution in sediment cores within a natural wetland polluted by acid mine drainage

Oscar E. Aguinaga [a, b], James F. T. Wakelin [c], Keith N. White [a], Andrew P. Dean [d], and Jon K. Pittman [a, *]

[a] School of Earth and Environmental Sciences, Faculty of Science and Engineering, The University of Manchester, Michael Smith Building, Oxford Road, Manchester M13 9PT, UK

[b] Departamento de Ingeniería, Facultad de Ciencias y Filosofía, Universidad Peruana Cayetano Heredia, Lima, Peru

[c] School of Environment, Education and Development, Faculty of Humanities, The University of Manchester, Arthur Lewis Building, Oxford Road, Manchester M13 9PL, UK

[d] Department of Natural Science, Faculty of Science and Engineering, Manchester Metropolitan University, Oxford Road, Manchester M1 5GD, UK

* Corresponding author.

E-mail address: jon.pittman@manchester.ac.uk (J. K. Pittman).

School of Earth and Environmental Sciences, Faculty of Science and Engineering, The University of Manchester, Michael Smith Building, Oxford Road, Manchester M13 9PT, UK. Tel: +44 161 275 5235.

Abstract

Natural recovery and remediation of acid mine drainage (AMD) reduces the generation of acidity and transport of trace elements in the runoff. A natural wetland that receives and remediates AMD from an abandoned copper mine at Parys Mountain (Anglesey, UK) was investigated for better understanding of the remediation mechanisms. Water column concentrations of dissolved Fe and S species, trace metal(loid)s and acidity decreased markedly as the mine drainage stream passed through the wetland. The metal(loid)s were removed from the water column by deposition into the sediment. Fe typically accumulated to higher concentrations in the surface layers of sediment while S and trace metal(loid)s were deposited at higher concentration within deeper (20 – 50 cm) sediments. High resolution X-ray fluorescence scans of sediment cores taken at three sites along the wetland indicates co–immobilization of Zn, Cu and S with sediment depth as each element showed a similar core profile. To examine the role of bacteria in sediment elemental deposition, marker genes for Fe and S metabolism were quantified. Increased expression of marker genes for S and Fe oxidation was detected at the same location within the middle of the wetland where significant decrease in SO_4^{2-} and Fe^{2+} was observed and where generation of particulate Fe occurs. This suggests that the distribution and speciation of Fe and S that mediates the immobilization and deposition of trace elements within the natural wetland sediments is mediated in part by bacterial activity.

Keywords: Acid mine drainage; Bacteria abundance; Metal deposition; Wetlands; X-ray fluorescence core scanning

1. Introduction

Metal and coal mining from abandoned and active mines release large amounts of contaminants such as trace metals (such as Cd, Cu and Zn) and metalloids (such as As) into the environment (Azapagic, 2004). These water streams from mines with

potentially toxic levels of acidity and metal ions are known as acid mine drainage (AMD), which is generated when sulfide ores such as pyrite are exposed to oxygen and water resulting in the oxidative dissolution of pyrite (Marchand et al., 2010). AMD is a serious environmental problem worldwide, which results in loss of habitats and biodiversity in freshwater ecosystems, and contaminates agricultural soil via polluted irrigation water (McKnight and Feder, 1984; Johnson and Hallberg, 2005; Zhuang et al., 2009; Dean et al., 2019). AMD pollution can therefore reduce the quality of food and water for human and animal consumption (Lin et al., 2005; Liu et al., 2012).

Typically used methods for AMD remediation include addition of alkaline materials to increase the water pH and accelerate the precipitation of metal ions (Coulton et al., 2003). Alternative sustainable passive methods such as the use of constructed wetlands have been shown to be a promising strategy for AMD remediation (Scholz and Lee, 2005; Babatunde et al., 2008). However, the long-term efficiency of using wetlands has been compromised by our limited understanding of the physicochemical and biotic mechanisms involved (Barton and Karathanasis, 1999; Valkanas and Trun, 2018). Study of natural wetland systems that have adapted over long time periods, often many decades, to tolerate AMD exposure may generate new insights for improving current passive treatment technologies. The ability of these natural wetlands to tolerate and eventually remediate AMD with very high acidity and high concentrations of dissolved metals is due to the action of the plants reducing water flow, mediating a degree of bulk metal extraction into biomass, enhancing input of organic carbon, including organic acids, and oxygen into the sediment to drive geochemical and biochemical reactions that lead to the formation of metal precipitates and alkalization (Beining and Otte, 1996; August et al., 2002; Jacob and Otte, 2003; Dean et al., 2013).

Prokaryotic microorganisms, including bacteria and archaea, have an important role in AMD remediation within wetlands. The activities of S and Fe oxidizing and reducing bacteria mediate the chemical reactions that release alkalinity (for example,

sulfate and Fe oxide reduction) and consume alkalinity (for example, Fe oxidation). In addition, metabolism of organic matter, which is abundant within the wetland, together with low oxygen availability, leads to reducing conditions that changes the distribution and speciation of metals within wetland sediments (Machel, 1989; Blgham et al., 1990; Fredrickson et al., 1998; Oueslati et al., 2019). The action of sulfate reducing bacteria contributes the most to metal removal in AMD-impacted environments, including wetlands (Johnson and Hallberg, 2005). In AMD affected wetlands, the sulfate reduction to hydrogen sulfide catalysed by these bacteria generates highly insoluble metal sulfide precipitates (Johnson and Hallberg, 2005). Specific genes related to S oxidation and reduction include *soxB*, which encodes a protein essential for thiosulfate bacterial oxidation and subsequent S oxidation (Epel et al., 2005), and the *dsrA* gene, which encodes a sulfite reductase responsible for dissimilatory sulfate reduction (Muyzer and Stams, 2008). In contrast, enzymatic mechanisms of Fe oxidation and reduction are less clear. However, specific species responsible for Fe metabolism have been identified, and these can be used as makers for Fe oxidation and reduction activities (Cummings et al., 2003; Heinzel et al., 2009). Bacterial activities related to Fe and S metabolism alongside abiotic mechanisms therefore results in increased metal precipitation within metal polluted environments resulting in the decrease in soluble metals in the water column and the continuous retention of metals within sediment layers. Marked shifts in metal distribution and bacteria populations can rapidly occur within short distance in AMD impacted environments (Valkanas and Trun, 2018).

The aim of this study was therefore to identify bacteria-mediated mechanisms of AMD attenuation in a wetland receiving and remediating AMD pollution. The study site for this investigation was the Afon Goch Wetland in Anglesey, UK that receives highly polluted AMD (pH 2.5) and removes >80% of dissolved Fe, Zn and Cu and increases pH to 5.5 within the first 700 m of the wetland system (Dean et al., 2013). Previous characterization of the Afon Goch wetland suggests that the remediation process is mediated by precipitation of metal(loid)s and accumulation of metal(loid)s in the

sediment, and due to a combination of chemical and biological processes (Boult, 1996; Batty et al., 2006; Dean et al., 2013; Aguinaga et al., 2018). However, the activities of specific bacteria related to S and Fe metabolism in association with a detailed analysis of sediment metal(loid) profiles are needed to begin to elucidate these biological processes. A combination of chemical measurements and bacterial activity was performed in this study to elucidate the geochemical and biological mechanisms underpinning the ability of the system to remediate AMD within a short distance. This will lead to a better understanding of the role of Fe and S bacteria-mediated transformation in AMD remediating wetland environments.

2. Materials and methods

2.1. Field site description and sampling details

The study site is a natural wetland that receives AMD pollution from an abandoned copper mine at Parys Mountain in Anglesey, UK (Fig. 1a). Drainage from Parys Mountain enters the Afon Goch river, and at 2.2 km downstream from the source the river enters a natural wetland that is approximately 2 km in length and has been shown to effectively remove metal(loid)s over the long term (Dean et al., 2013). Three sample locations along the wetland were analyzed during 2017 and 2018 (Fig. 1b and c). Site W1 was located at ~500 m from the AMD source and is where the attenuation process starts. Site W2 was located in the zone where the large decrease in acidity and dissolved metal(loid) concentration have previously been observed, while site W3 was located in the lower reaches of the wetland where pollution levels are significantly reduced (Dean et al., 2013; Aguinaga et al., 2018).

In situ water measurements of pH were performed using a portable pH meter (Hanna Instruments, UK). Measurement of Fe^{2+}, sulfate and sulfide concentrations was carried out by using the 1,10-Phenanthroline, Methylene Blue and SulfaVer 4 methods, respectively (Rice et al., 2012), employing a DR900 Multiparameter Portable

Colorimeter (Hach, USA). For dissolved metal(loid) analysis a known volume of surface water (~2 cm depth) was filtered through a 0.45 µm cellulose acetate filter, and preserved by addition of nitric acid to a final concentration of 2%. The filters were retained for analysis of metal(loid) particulates. Five replicate water samples were taken in each of the three locations.

Sediment core samples were taken to a depth of 50 cm using a Russian corer (Van Walt, UK). Twenty cores taken during 2017 from site W2 were extracted from un-vegetated river sediment (5 replicate cores), and from sediments within plant stands of *Eriophorum angustifolium*, *Juncus* sp. and *Phragmites australis* (5 replicate cores for each plant stand). Visual inspection of the cores from the vegetated stands revealed three distinct zones, and hence each core was separated into a surface layer (typically 0 – 10 cm) containing larger soil particles and plant debris, a middle layer (typically 10 – 20 cm) characterized by a red-brown color with compacted ochre, and a bottom layer (typically 20 – 50 cm) of black mud. The distinct middle band of sediment was absent from the riverbed cores. Therefore for subsequent analyses cores were split into just two depth layers; a top layer (0 – 20 cm) and a bottom layer (20 – 50 cm). These sediment layers were transferred into 50 mL polypropylene tubes for subsequent metal(loid) extraction and analysis by inductively coupled plasma atomic emission spectroscopy (ICP-AES) or RNA extraction for subsequent gene expression measurement. LifeGuard soil RNA preservation solution (Qiagen, USA) was used to stabilize the microbial RNA at ambient temperature during field sampling. The solution was added to the samples to be used for RNA analysis. Once in the laboratory, samples were frozen at -20 °C until RNA extraction was performed.

A further 24 cores were taken during 2018 from site W1, W2 and W3 from sediments within *Juncus* sp. plant stands only (8 replicate cores per site). Five of the replicate cores from each site were divided into top layer (0 – 20 cm) and bottom layer (20 – 50 cm). These sediment layers were transferred into 50 mL polypropylene tubes for subsequent metal(loid) analysis by ICP-AES or RNA extraction for subsequent gene

expression measurement. The remaining three replicate sediment cores were used for X-ray fluorescence (XRF) core scanning. These cores were placed in PVC tubes and wrapped with protective film for transportation to the laboratory. Samples from these cores were then used for C and N measurements.

2.2. XRF core scanning

High-resolution profiles of element concentrations were determined along 9 sediment cores (3 replicate cores each for sites W1, W2 and W3) via non-destructive, XRF spectrometry using an ITRAX core scanner (School of Environment, Education and Development, University of Manchester). Prior to analysis, each core was prepared by ensuring that the surfaces were completely flat using a roller. The X-rays used to irradiate the cores were generated by a 3 kW Mo-tube. A step size of 1 mm and a count time at each step of 20 s were selected. Data for Fe, S, Zn, Cu, Mn, Al, As and Pb was obtained from the scans and expressed as total counts per s (CPS). To transform CPS into element concentrations (mmol g^{-1}), the total concentration of each element from selected 10 mm core sections was determined by ICP-AES following acid digestion (as detailed in Section 2.3 below). Linear regression between CPS and ICP-AES values was performed (Fig. S1) and used to convert CPS values to concentrations (mmol g^{-1}).

2.3. ICP-AES analysis

Dissolved metal(loid) concentrations were determined by ICP-AES analysis of the acidified filtered water samples. Particulate metal(loid) concentrations were determined by drying the filter paper at 80 °C for 48 h, followed by digestion in the filter paper and retained particulates in 67% ultra-pure nitric acid for 4 h at 70°C. Sediment samples were homogenized and dried at 80 °C for 48 h, and passed through a 250 µm mesh stainless steel sieve. Sediments were then digested in 67% ultra-pure nitric acid at 70 °C, which extracts all adsorbed and organically-bound metal(loid)s, and the

digests were diluted to 2% acid in deionized Milli-Q water (Millipore, UK). Samples were analyzed for Fe, S, Zn. Cu, Mn, Al, As, Pb by ICP-AES using a Perkin-Elmer Optima 5300. Certified Reference Standard TM25.5 was used and all samples were calibrated using a matrix-matched serial dilution of Specpure multi-element plasma standard solution 4 (Alfa Aesar, UK) set by linear regression, and only results with a relative standard deviation < 20% were considered.

2.4. Sediment core C and N analysis

For analysis of Total C (TC) and Total N (TN) content, 5 g sediment samples were taken at 10 cm intervals along each replicate core, dried at 80 °C for 24 h and disaggregated using a Mixer Mill MM 400 (Retsch, Germany). Samples were analyzed by combustion using an Elemental Vario EL elemental analyzer (Elementar Analysensysteme, Germany) following the manufacturer's instructions. For the determination of water-extractable C and N, 5 g of sediment was taken at 10 cm intervals along each core and extracted in 35 mL of Milli-Q water for 10 min using an orbital shaker. Extracts were then filtered using Whatman no.1 filters (Camlab, UK). Total inorganic C (IC) concentrations from the extracts were measured using a non-dispersive infra-red gas analyzer (Shimadzu SSM-5000A, Shimadzu, UK). The dissolved organic C (DOC) fraction was determined by subtracting IC values from TC values. Concentrations of dissolved nitrate and ammonium were determined by colorimetric detection using an AutoAnalyser 3 HR (Seal Analytical, UK) following the manufacturer's instructions. Dissolved organic N (DON) was determined as the difference between TN and the inorganic fractions (nitrate and ammonium).

2.5. Microbial gene expression

RNA was extracted from 4 g of surface and bottom layer sediment from five replicate core samples from each site using a RNeasy PowerSoil Total RNA kit (Qiagen, USA). To remove genomic DNA, RNA samples were treated with DNAse I

(New England Biolabs, UK) following the manufacturer's instructions. RNA was quantified using a Nano-drop 3300 (Thermo-Scientific, USA). Reverse transcription of RNA was performed using SuperScript II Reverse Transcriptase (Thermo-Scientific, USA) following the manufacturer's instructions. Random hexamers (Thermo-Scientific, USA) were used as primers for synthesis of cDNA. Gene expression analysis by quantification of the resulting cDNA was performed by quantitative real-time PCR (qPCR) for six marker genes using specific primer sets (Table S1). Each reaction consisted of 10 µL of SensiFAST SYBR Hi-Rox mix, 0.8 µL of each forward and reverse primers (10 µM), 0.5 µL of cDNA, in a final reaction volume made up to 20 µL with nuclease-free water. Samples were run on a Step One Plus Real Time PCR system (Applied Biosystem, UK) with SYBR Green Rox detection program. Standard curves for each set of primers were obtained via a series of 1 in 10 dilutions of cDNA from samples with a known cDNA concentration, and the concentration of cDNA transcripts were calculated by absolute quantification. Analysis was performed on five independent biological replicates for each sample site. Reactions using RNA as template were included as a control of possible genomic DNA contamination, while negative controls consisted of no template nucleotide.

2.6. Statistical analysis

Statistical analysis of environmental parameters and gene expression data were determined by one-way analysis of variance (ANOVA) using a Tukey post-hoc test performed using GraphPad Prism 7.

3. Results and discussion

3.1. Acidity and metal(loid) attenuation along the AMD stream through the wetland

In situ measurements of pH in surface waters from sites W1, W2 and W3 show a significant decrease in acidity ($P < 0.05$) from the upper reaches of the wetland

nearest the source (pH 2.5) to the end of the wetland (pH 5.8) (Fig. 2a). This confirms the acidity attenuation detected over 20 years of monitoring at this site (Dean et al., 2013; Aguinaga et al., 2018). Significant differences in Fe and S concentrations were also observed across the wetland sites. On entering the wetland, levels of particulate and dissolved Fe were similar (Fig. 2b – c) with median values of 0.08 mM and 0.12 mM, respectively. There was a mean 3.9-fold increase in particulate Fe at site W2, although due to large variation in replicate samples this apparent increase is not statistically significant. Site W2 is the area of the wetland previously identified to be where the most marked changes in water chemistry occur (Dean et al., 2013; Aguinaga et al., 2018). Moreover, site W2 has greater plant diversity comprised of different wetland plant stands, which may lead to variation in carbon release and suspended organic matter, potentially explaining the differences in particulate Fe concentration observed. Further along the wetland (site W3) the particulate Fe had fallen significantly by 11.8-fold. Dissolved Fe decreased along the wetland (Fig. 2c) with a 8.9-fold decrease ($P < 0.05$) between sites W1 and W3. Both Fe^{2+} and Fe^{3+} decreased along the wetland with Fe^{3+} present at concentrations typically 3 times that of Fe^{2+} (Fig. 2d). The reduction in dissolved Fe and increase in particulate Fe as in the middle of the wetland (W2) is typical of a transition from soluble Fe^{2+} to aggregates of Fe^{3+} in the form of Fe^{3+} oxides and hydroxides (Boult et al., 1994; Dean et al., 2013; Aguinaga et al., 2018). However, the profile of particulate Fe across the wetland (Fig. 2b) did not correlate with changes in Fe^{3+} (Fig. 2d), suggesting that other mechanisms are involved in Fe aggregation and soluble Fe removal from the water column.

Particulate S showed no significant difference and was present at all sites at concentrations between 0.28 – 0.87 mM (Fig. 2e). In contrast, dissolved S showed a significant 26.8-fold decrease ($P < 0.05$) from 1.9 to 0.07 mM between sites W1 and W2, while sulfate concentration showed a 10.2-fold decrease ($P < 0.05$) (Fig. 2f – g). Sulfide also showed a significant 4.2-fold decrease ($P < 0.05$) along the wetland (Fig. 2h). Sulfate is the main S compound produced during the oxidation of pyrite and

277 subsequent generation of AMD (Evangelou and Zhang, 1995). The decrease in sulfate
278 and dissolved S suggests that most of the S is being removed in the form of sulfate.
279 The sulfate that precipitates into the sediments can be reduced and immobilized as
280 sedimentary pyrite (Berner, 1985). The key process facilitating the removal of sulfate
281 from the water column is its reduction and transformation to hydrogen sulfide (Akcil and
282 Koldas, 2006). However, sulfide levels were much lower than the other S compounds
283 measured. One explanation is that elemental S and compounds such as sulfite and
284 thiosulfate, which are also susceptible to chemical and biological oxidation (Auernik
285 and Kelly, 2008; Amouric et al., 2009), are present in significant quantities.
286 Measurement of sulfide is important as this compound is capable of binding to and co-
287 precipitating trace metal(loid)s (Machemer and Wildeman, 1992). However, large
288 amounts of sulfide were not detected in the water column, possibly due to rapid
289 precipitation of metal sulfides close to the source in the upper reaches of the wetland.
290 A significant decrease ($P < 0.05$) in dissolved concentrations of Zn, Mn and Al
291 from the upper site W1 to sites W2 and W3 was observed (Fig. S2), confirming the
292 rapid attenuation of these metal(loid)s as the AMD stream flows through the first km of
293 the wetland (Dean et al., 2013; Aguinaga et al., 2018). This suggests that dissolved Zn,
294 Mn and Al concentrations can decrease due to metal sulfide precipitation, binding
295 to Fe^{3+} compounds, and the formation of oxide compounds, which is particularly the
296 case for Al and Mn (Scheinost, 2005). Concentrations of dissolved Cu, As and Pb
297 showed no significant change at any site along the wetland (Fig. S2), possibly due to
298 differences in chemical speciation between these metal(loid)s and Zn, Mn and Al.
299 Furthermore, no significant variation in particulate trace metal(loid)s was detected (Fig.
300 S3). This infers that metal(loid) partitioning differs depending on metal(loid) type and
301 total concentration. Difference in precipitation rates depending on the metal(loid) have
302 been previously observed due to differences in metal(loid) adsorption capacity to
303 organic compounds in constructed wetlands and metal(loid) selective interactions with
304 biogenic sulfide produced by bacteria from AMD environments (Jameson et al., 2010).

305 Difference in metal(loid)s susceptibility to sulfide interaction and pyrite formation can
306 also explain differences in precipitation rates. For example, Cu and Pb are moderately
307 sufidized (11 – 16% of the reactive fraction) compared to other extensively sulfidized
308 metals in freshwater sediments (Huerta-Diaz et al., 1998).
309
310 *3.2. Deposition of metal(loid)s in sediments*
311 The rapid decrease in dissolved concentrations of Zn, Mn, Al, Fe and S
312 between sites W1 and W2 suggests substantial deposition into the sediments within
313 the middle of the wetland. Metal(loid) concentrations at different sediment depths at
314 site W2 were analyzed to obtain further insight into metal(loid) immobilization
315 processes. The wetland had stands of different wetland plant species, with *Eriophorum*
316 *angustifolium*, *Juncus* sp. and *Phragmites australis* being the dominant species. To
317 examine possible differences in metal(loid) distribution due to different plant species,
318 replicate cores were taken from different plant stands. Furthermore, to examine
319 possible differences in metal(loid) distribution arising from the absence of vegetation,
320 replicate cores were taken from the riverbed. As described in Section 2.1, visual
321 inspection of the cores from the vegetated stands revealed three distinct layers. The
322 layers showed difference in metal(loid) concentration (Fig. 3). Fe concentrations were
323 significantly lower ($P < 0.05$) in the bottom layer compared to surface and/or middle
324 layer for all samples (Fig. 3a). In contrast, S and trace metal(loid)s show higher
325 concentrations in the bottom layer (Fig. 3b – h). Concentrations of elements in the
326 sediment layer surrounding the roots (surface layer) of different plant species showed
327 no significant differences. Furthermore, there was no significant difference between
328 metal(loid) deposition pattern in the presence or absence of plants, and the absence of
329 plants only had a significant affect ($P < 0.05$) for Cu within bottom layer of the core (Fig.
330 3d). In contrast, a previous study of cores within the Afon Goch wetland suggested that
331 the presence of vegetation was important since it lead to increased porewater

metal(loid) concentrations, potentially due to higher evapotranspiration rates (Batty et al., 2006).

As difference in the depth distribution of Fe and S were observed at site W2, the analysis was extended to assess core samples at all sites. Since no significant differences in metal(loid) distribution were observed within the first 20 cm of the cores at W2 (between surface and middle layers) or between different plant species cores, subsequent cores were only taken from *Juncus* stands, as this species was present at all sample sites, and cores were divided into a top layer (0 – 20 cm) and a bottom layer (20 – 50 cm). Fe showed a significantly lower ($P < 0.05$) concentration in the top layer compared to the bottom layer at site W2 but there was no significant difference with depth at the other sites (Fig. 4a). In contrast, S concentration was lower in the top layer compared to the bottom layer at all sites, with a significant difference ($P < 0.05$) at sites W1 and W3 (Fig. 4b). The depth profile of other metal(loid)s was also investigated. Surface core concentrations of Cu, Mn, Al and Pb were significantly lower ($P < 0.05$) than in the bottom layer at site W1 (Fig. 4). Zn was present at higher concentrations in the upper sediment layer at all three sites while As showed no significant difference between layers at any site. Cu was the only trace metal that showed significant changes ($P < 0.05$) in the bottom layer with lower concentrations at W2 and W3 compared to W1 (Fig. 4d). These results suggest retention of Fe in the upper layer while S and trace metal(loid)s are more prone to accumulate in the bottom layers of sediment; however, metal(loid) type and distance from the source of the AMD also influenced elemental distribution within the sediments.

3.3. High resolution analysis of core sediments

Since analysis of the sediment cores revealed marked differences in depth distribution of various elements, a more detailed spatial analysis was performed. Spatial changes in metal(loid) distribution, particularly with depth, can be elucidated at high resolution along the sediment cores by XRF core scanning technology, which has

previously been used to detect and monitor sediment pollution from mining and industry sites (Rodríguez-Germade et al., 2014; Croudace et al., 2015; Rodríguez-Germade et al., 2015). XRF core scanning was carried out at 1 mm resolution along the cores from each of the three sites within the wetland. Scans showed that the Fe concentration was consistently high along all cores, which varied between 0.9 – 1.8 mmol g^{-1}; however a slight decrease in Fe concentration in deeper layers was observed (Fig. 5). This was particularly evident in W2 cores where there was a marked reduction in Fe deposition at 30 – 35 cm depth. In contrast, S showed increased concentration with depth. The sediment at site W1 showed the highest values of S nearer to the surface (with a peak at 10 cm depth), while the peak deposition of S at sites W2 and W3 was at lower depths, at 30 cm and 40 cm, respectively.

In anoxic environments significant accumulation of S typically occurs at the surface due to sedimentation of sulfide-rich suspended matter (Zwolsman et al., 1993). However, since S was observed to accumulate in deeper layers within the wetland sediments this suggests oxygenation of the upper sediment, potentially due to oxygen release via the roots of the wetland plants (Colmer, 2003). Potentially the oxic surface layer is influencing the precipitation of sulfide in deeper layers. While the wetland was mainly populated by species of *Juncus*, site W2 had more diversity of vegetation including *P. australis* and *E. angustifolium*. It is known that plant roots have different oxygen loss rates depending on their growth rate, which varies between species (Lai et al., 2012). Therefore the greater plant diversity at site W2 may result in a deeper oxic layer, which may enhance the accumulation of sulfide to deeper anoxic layers. The presence of oxygen will generate ideal redox conditions for aerobic bacteria that use oxygen as an electron acceptor in the oxidation of substrates such as Fe and S (discussed below in Section 3.4). Such differences in surface sediment S concentration compared to deeper sediments have also been seen in paddy field cores impacted by AMD (Yang et al., 2016). It has been suggested that the deposition of sulfate onto AMD-affected sediments is often in the form of the iron-oxyhydroxysulphate mineral

388 schwertmannite, which is mediated by low pH values and high Fe concentrations
389 (Chen et al., 2015).
390 The profile of Fe within the sediment cores from each site did not correlate with
391 trace metal(loid)s including Zn and Cu, suggesting that interaction of these metal(loid)s
392 with Fe oxyhydroxides may not be an important process. In contrast, there were
393 similarities in S, Zn and Cu distribution (Fig. 5), with peaks of these elements observed
394 in similar positions at ~10 cm and ~20 cm in W1 cores, at ~30 cm in W2 cores, and at
395 ~40 cm in W3 cores. This suggests that the mobility of these trace metal(loid)s may be
396 modulated by S, and given the elevated concentrations of reduced S compounds in
397 AMD environments, this is likely to be due to immobilization of Cu and Zn as sulfides
398 (Yang et al., 2016). Experiments using mixed metal(loid) solutions for generation of
399 metal sulfide compounds under laboratory conditions have shown that Fe-sulfide
400 complexes can be dissociated at pH below 5 while Cu and Zn formed stronger sulfide
401 complexes that require higher acidity to dissociate (Luther et al., 1996). A strong
402 correlation between the vertical distribution of Cu and Zn has been previously observed
403 in sediment cores from other AMD impacted wetlands (von der Heyden and New,
404 2004) and metal(loid) polluted estuaries (Zwolsman et al., 1993). In both cases,
405 sediment dating revealed that similar distribution patterns were an indicator of
406 similarities in pollution history such as the same source and/or deposition rate. In this
407 study, Fe showed no accumulation spike despite redox zonation of sediments, and no
408 correlation with other sediment metal(loid)s was observed. Previous work in an AMD
409 impacted natural wetland revealed that the sedimentary source of Fe could change
410 along the wetland (von der Heyden and New, 2004). Here we suggest that the ratio
411 between Fe and trace metal(loid)s entering the wetland varies with time and therefore
412 result in different accumulation patterns. This suggests that even though metal(loid)
413 distribution can be explained by chemical and biological mechanisms, environmental
414 changes with time such as pollution levels and flux need to be understood. For
415 example, it is known that AMD discharges entering the Afon Goch wetland has varied

with time, thereby creating variations in the water level and oxygen concentrations which generate short–term fluctuations in redox conditions and therefore changes in sedimentation rates especially for redox sensitive metals such as Fe and Mn (Vranken et al., 1990). Furthermore, transient oxygenation can remobilize some metal(loid)s (Tribovillard et al., 2006). Large-scale changes such as significant decrease in metal(loid) inflow due to a substantial lowering of the water table (Dean et al., 2013) can also influence horizontal accumulation patterns along sediment depth.

The XRF core analysis also showed variation between the profiles of Mn, Al, As and Pb (Fig. S4). Al showed a stable profile (~1 mmol g^{-1}) with depth, while Mn, As and Pb showed considerable variation both at depths and between sites. However, Al is at the limit of ITRAX detection due to its low atomic weight and hence concentrations can be underestimated (Rothwell et al., 2006). The profiles of Al, Mn and As showed different patterns when compared to the previous bulk layer analysis. Previous studies have demonstrated that an XRF core profile needs to be carefully interpreted in sediments with differing water content (Tjallingii et al., 2007) and large variations in organic matter and carbon concentration (Chawchai et al., 2016). Furthermore, mobilization of trace metal(loid)s such as Cu and As can be influenced by dissolved organic matter concentration in the soil solution (Kalbitz and Wennrich, 1998). However, in this study, no significant variations of TC or DOC and TN or DON along the sediment cores were observed (Fig. S5), and no significant correlation between DOC, DON, and trace metal(loid)s with depth was observed. This suggests that decay of substantial amounts of organic material from the wetland plants over a long time period has led to an excess of organic C and N throughout the sediment.

3.4. Bacterial activity in the surface and bottom layers of the wetland sediments

In order to investigate the potential role of bacteria in mediating metal(loid) distribution within the sediments, the expression patterns of specific bacteria marker genes were measured in surface and bottom sediment samples from cores taken

444 within stands of *Juncus* sp. The 16S rRNA abundance of total bacteria did not show
445 any significant change along the wetland, although a significant difference ($P < 0.05$)
446 with depth was observed at sites W1 and W2 (Fig. 6a). More specifically, no significant
447 partitioning in the expression of *Geobacter* spp. 16S rRNA, an Fe reduction marker,
448 was observed in the W2 and W3 cores but a significant reduction ($P < 0.05$) was seen
449 in *Geobacter* spp. abundance in the bottom layer of W1 cores compared to W2 and W3
450 cores (Fig. 6b). Anaerobic Fe metabolism from bacteria related to the *Geobacter* taxa
451 has been previously observed (Coates et al., 2001) and utilization of Fe minerals in
452 anaerobic sediments by these bacteria has been described (Adams et al., 2007).
453 Two sets of Fe oxidation markers were tested; abundance of *Gallionella* spp.
454 and related taxa, and abundance of *Ferrovum* spp. and related taxa. Abundance of
455 "*Gallionella* and relatives" 16S rRNA showed no significant differences between any of
456 the sediment layers or sites (Fig. 6c). In contrast, the most notable result was the
457 significantly higher abundance ($P < 0.05$) of 16S rRNA of "*Ferrovum* and relatives"
458 within the surface layer of W2 cores compared to the other samples (Fig. 6d). Strains
459 of *Ferrovum myxofaciens* capable of catalyzing the oxidative dissolution of pyrite were
460 previously isolated from the Parys Mountain mine site (Johnson et al., 2014). The
461 presence of *Ferrovum* at site W2 demonstrates that this taxa can also thrive in the
462 surrounding wetland under less extreme conditions and suggests that its abundance
463 coincides with an improvement in water quality within the middle area of the wetland.
464 Even though no specific functional gene related to Fe metabolism was measured, the
465 analysis of different obligate Fe metabolizing bacteria suggest that Fe oxidation is an
466 important metal(loid) immobilizing mechanism along the Afon Goch wetland.
467 The mRNA transcript abundance of the *soxB* gene, a marker of S oxidation, and
468 the *dsrA* gene, a marker of sulfate reduction, were measured. The surface sediment
469 layer at site W2 had significantly increased ($P < 0.05$) *soxB* expression (Fig. 6e), which
470 was expected within such as oxygenated zone. A similar increase in expression of the
471 *soxB* gene was associated with the oxidation of thiosulfate to sulfate using the SoxCD

enzyme complex in a terrestrial sulfidic spring (Headd and Engel, 2013). In contrast, expression of *dsrA* showed no difference with depth at any of the sites; however, the amount of *dsrA* transcript in the surface layer of W1 and W2 cores were significantly higher ($P < 0.05$) than in the W3 cores (Fig. 6f). A decrease in dissimilatory sulfate reduction activity can be explained by depletion of sulfate when at site W3. To further understand the partitioning of S oxidation along the wetland, future studies should measure activities of other S compounds beside sulfate and sulfide. Furthermore, higher resolution gene expression analysis that is equivalent to the resolution of metal(loid) profiling by XRF core analysis, will allow a more detailed understanding and association of the roles of the microbial communities throughout the sediment profile.

The increased abundance of the functional gene *soxB* and the "*Ferrovum* and relatives" 16S rRNA gene that was observed in the W2 core surface sediment was further evaluated in surface sediments associated with different plant species and within the un-vegetated river sediments. This was to determine if there was any association between the plants species within the wetland and the presence of *Ferrovum*, and the expression of the *soxB* gene. Expression of *soxB* showed no significant difference between samples (Fig. S6a). It is known that the *soxB* gene encodes part of a periplasmic thiosulphate oxidizing complex that is widespread among different phylogenetic groups (Friedrich et al., 2001; Petri et al., 2001). This diversity has also been observed in thiosulphate oxidizing bacteria expressing *soxB* in rhizosphere soil from different plant species (Ghosh et al., 2006; Anandham et al., 2008; Li et al., 2014). Ubiquitous expression of *soxB* can thus explain the similar expression levels observed in different wetland plant species and non-vegetated areas. In contrast "*Ferrovum* and relatives" 16S rRNA showed significant increased ($P < 0.05$) abundance in the vegetated sediments compared to the river sample, yet there was no significant difference between the different plant species (Fig. S6b). This suggests that wetland vegetation plays an important role in maintaining the abundance of *Ferrovum*

spp. within the middle of the wetland, and the presence of wetland plants therefore helps facilitate bacterial mediated Fe oxidation.

Together these results allow us to propose a model indicating the importance of the wetland vegetation in association with microbial communities in driving changes in metal(loid) distribution with sediment depth (Fig. 7). (1) Oxygenation of the water column and upper sediment layers due to oxygen release from plant roots mediates dissolved trace metal(loid) oxidation. (2) This is followed by deposition to deeper sediment layers. In an organic-rich wetland sediment, where biological oxygen demand is high, oxygen concentration rapidly reduces along the depth of the sediment core giving rise to an oxygen gradient with an oxic zone in surface layer and an anoxic zone in bottom layers (Lüdemann et al., 2000; Ratering and Schnell, 2000). (3) Anoxic layers generate sulfide compounds that can bind trace metals such as Cu and Zn, as seen by Cu-S and Zn-S associations in deeper sediment layers. In addition to sulfide, Fe^{3+} and organic carbon can bind with trace metals within the sediments. (4) Carbon derived from the wetlands plants will maintain bacterial communities. Increased abundance of obligate Fe oxidizing bacteria in upper sediment suggests increased oxidation of Fe^{2+}. S oxidation activities were also observed in upper sediment. (5) Dominance of sulfate reducing bacteria and rapid decrease in sulfate levels also suggests microbial derived generation of sulfide. Together these activities remove metal(loid)s from the water column, as evidenced by a decrease in soluble metal(loid) levels along the wetland.

4. Conclusions

It has been suggested that the sediments within natural wetlands are an important sink for metal deposition, particularly in the form of Fe^{3+} compounds (Boult et al., 1994; Dean et al., 2013). Detailed analysis of metal distributions within wetland sediments confirmed that the variation in metal distribution with depth and the potential changes in mobilization due to environmental conditions is part of a complex dynamic of metal chemistry in wetlands. It was observed that while Fe was typically partitioned

in the surface sediment, S and trace metals accumulated in deeper layers. High-resolution analysis of sediment cores suggests a co-immobilization of S, Cu and Zn at greater sediment depths due to possible binding of the trace metals to sulfide compounds. However, the timeframes within which these metals were deposited within the wetland sediments remain unclear. Previous work has highlighted the importance of bacteria in the wetland remediation process and the crucial role of wetlands in maintaining microbial diversity and activity (Aguinaga et al., 2018). In this present study, further insights into the remediation mechanisms occurring along the Afon Goch wetland were provided by an examination of the sediment microbiology and its association with metal distribution and speciation. Higher S oxidation and increase in the abundance of obligate Fe oxidizing bacteria within the first 20 cm of the sediment depth coincided with changes in trace metal chemistry and Fe and S speciation. This suggests that bacterial metabolism enhances the Fe and S transformations that lead to the rapid metal attenuation within a short distance from the source of the AMD pollution.

Acknowledgements

This work was financially supported in part by PhD scholarship funding (to OEA) from the National Fund for Scientific, Technological Development and Technological Innovation (FONDECYT) of Peru. We acknowledge the assistance of Paul Lythgoe for ICP-AES analysis, Thomas Bishop and John Moore for ITRAX core scanning, Debbie Ashworth for carbon and nitrogen measurements, and Mariela Aguilera for assistance with field sampling.

555 **References**

556

557 Adams, L., Harrison, J., Lloyd, J., Langley, S., Fortin, D., 2007. Activity and diversity of
558 Fe (III)-reducing bacteria in a 3000-year-old acid mine drainage site analogue.
559 Geomicrobiol. J. 24, 295-305.

560 Aguinaga, O.E., McMahon, A., White, K.N., Dean, A.P., Pittman, J.K., 2018. Microbial
561 community shifts in response to acid mine drainage pollution within a natural wetland
562 ecosystem. Front. Microbiol. 9, 1445.

563 Akcil, A., Koldas, S., 2006. Acid Mine Drainage (AMD): causes, treatment and case
564 studies. J. Clean. Prod. 14, 1139-1145.

565 Amouric, A., Appia-Ayme, C., Yarzabal, A., Bonnefoy, V., 2009. Regulation of the iron
566 and sulfur oxidation pathways in the acidophilic *Acidithiobacillus ferrooxidans*. Adv.
567 Mat. Res. 71-73, 163-166.

568 Anandham, R., Indiragandhi, P., Madhaiyan, M., Ryu, K.Y., Jee, H.J., Sa, T.M., 2008.
569 Chemolithoautotrophic oxidation of thiosulfate and phylogenetic distribution of sulfur
570 oxidation gene (soxB) in rhizobacteria isolated from crop plants. Res. Microbiol. 159,
571 579-589.

572 Auernik, K.S., Kelly, R.M., 2008. Identification of components of electron transport
573 chains in the extremely thermoacidophilic crenarchaeon *Metallosphaera sedula*
574 through iron and sulfur compound oxidation transcriptomes. Appl. Environ. Microbiol.
575 74, 7723-7732.

576 August, E.E., McKnight, D.M., Hrncir, D.C., Garhart, K.S., 2002. Seasonal variability of
577 metals transport through a wetland impacted by mine drainage in the Rocky
578 Mountains. Environ. Sci. Technol. 36, 3779-3786.

579 Azapagic, A., 2004. Developing a framework for sustainable development indicators for
580 the mining and minerals industry. J. Clean. Prod. 12, 639-662.

581 Babatunde, A., Zhao, Y., O'Neill, M., O'Sullivan, B., 2008. Constructed wetlands for
582 environmental pollution control: a review of developments, research and practice in
583 Ireland. Environ. Int. 34, 116-126.

584 Barton, C., Karathanasis, A., 1999. Renovation of a failed constructed wetland treating
585 acid mine drainage. Environ. Geol. 39, 39-50.

586 Batty, L.C., Baker, A.J.M., Wheeler, B.D., 2006. The effect of vegetation on porewater
587 composition in a natural wetland receiving acid mine drainage. Wetlands 26, 40-48.

588 Beining, B.A., Otte, M.L., 1996. Retention of metals originating from an abandoned
589 lead-zinc mine by a wetland at Glendalough, Co Wicklow. Biol. Environ. 96B, 117-126.

590 Berner, R.A., 1985. Sulphate reduction, organic matter decomposition and pyrite
591 formation. Phil. Trans. R. Soc. A 315, 25-38.

592 Blgham, J.M., Schwertmann, U., Carlson, L., Murad, E., 1990. A poorly crystallized
593 oxyhydroxysulfate of iron formed by bacterial oxidation of Fe(II) in acid mine waters.
594 Geochim. Cosmochim. Acta 54, 2743-2758.

595 Boult, S., 1996. Fluvial metal transport near sources of acid mine-drainage:
596 Relationships of soluble, suspended and deposited metal. Mineral. Mag. 60, 325-335.

597 Boult, S., Collins, D.N., White, K.N., Curtis, C.D., 1994. Metal transport in a stream
598 polluted by acid mine drainage—the Afon Goch, Anglesey, UK. Environ. Pollut. 84,
599 279-284.

600 Chawchai, S., Kylander, M.E., Chabangborn, A., Löwemark, L., Wohlfarth, B., 2016.
601 Testing commonly used X-ray fluorescence core scanning-based proxies for organic-
602 rich lake sediments and peat. Boreas 45, 180-189.

603 Chen, M., Lu, G., Guo, C., Yang, C., Wu, J., Huang, W., Yee, N., Dang, Z., 2015.
604 Sulfate migration in a river affected by acid mine drainage from the Dabaoshan mining
605 area, South China. Chemosphere 119, 734-743.

606 Coates, J.D., Bhupathiraju, V.K., Achenbach, L.A., Mclnerney, M., Lovley, D.R., 2001.
607 *Geobacter hydrogenophilus*, *Geobacter chapellei* and *Geobacter grbiciae*, three new,
608 strictly anaerobic, dissimilatory Fe (III)-reducers. Int. J. Syst. Evol. Microbiol. 51, 581-
609 588.

610 Colmer, T.D., 2003. Long-distance transport of gases in plants: a perspective on
611 internal aeration and radial oxygen loss from roots. Plant, Cell Environ. 26, 17-36.

612 Coulton, R., Bullen, C., Hallett, C., 2003. The design and optimisation of active mine
613 water treatment plants. Land Contam. Reclamat. 11, 273-280.

614 Croudace, I.W., Romano, E., Ausili, A., Bergamin, L., Rothwell, R.G., 2015. X-ray core
615 scanners as an environmental forensics tool: A case study of polluted harbour
616 sediment (Augusta Bay, Sicily). In: Croudace, I.W., Rothwell, R.G. (Eds.). Micro-XRF
617 Studies of Sediment Cores: Applications of a non-destructive tool for the environmental
618 sciences. Springer Netherlands, Dordrecht, pp. 393-421.

619 Cummings, D.E., Snoeyenbos-West, O.L., Newby, D.T., Niggemyer, A.M., Lovley,
620 D.R., Achenbach, L.A., Rosenzweig, R.F., 2003. Diversity of Geobacteraceae species
621 inhabiting metal-polluted freshwater lake sediments ascertained by 16S rDNA
622 analyses. Microb. Ecol. 46, 257-269.

623 Dean, A.P., Hartley, A., McIntosh, O.A., Smith, A., Feord, H.K., Holmberg, N.H., King,
624 T., Yardley, E., White, K.N., Pittman, J.K., 2019. Metabolic adaptation of a
625 *Chlamydomonas acidophila* strain isolated from acid mine drainage ponds with low
626 eukaryotic diversity. Sci. Total Environ. 647, 75-87.

627 Dean, A.P., Lynch, S., Rowland, P., Toft, B.D., Pittman, J.K., White, K.N., 2013.
628 Natural wetlands are efficient at providing long-term metal remediation of freshwater
629 systems polluted by acid mine drainage. Environ. Sci. Technol. 47, 12029-12036.

630 Epel, B., Schäfer, K.-O., Quentmeier, A., Friedrich, C., Lubitz, W., 2005. Multifrequency
631 EPR analysis of the dimanganese cluster of the putative sulfate thiohydrolase SoxB of
632 *Paracoccus pantotrophus*. J. Biol. Inorg. Chem. 10, 636-642.

633 Evangelou, V., Zhang, Y., 1995. A review: pyrite oxidation mechanisms and acid mine
634 drainage prevention. Crit. Rev. Environ. Sci. Technol. 25, 141-199.

635 Fredrickson, J.K., Zachara, J.M., Kennedy, D.W., Dong, H., Onstott, T.C., Hinman,
636 N.W., Li, S.-m., 1998. Biogenic iron mineralization accompanying the dissimilatory
637 reduction of hydrous ferric oxide by a groundwater bacterium. Geochim. Cosmochim.
638 Acta 62, 3239-3257.

639 Friedrich, C.G., Rother, D., Bardischewsky, F., Quentmeier, A., Fischer, J., 2001.
640 Oxidation of reduced inorganic sulfur compounds by bacteria: emergence of a common
641 mechanism? Appl. Environ. Microbiol. 67, 2873-2882.

642 Ghosh, W., Mandal, S., Roy, P., 2006. *Paracoccus bengalensis* sp. nov., a novel
643 sulfur-oxidizing chemolithoautotroph from the rhizospheric soil of an Indian tropical
644 leguminous plant. Syst. Appl. Microbiol. 29, 396-403.

645 Headd, B., Engel, A.S., 2013. Evidence for niche partitioning revealed by the
646 distribution of sulfur oxidation genes collected from areas of a terrestrial sulfidic spring
647 with differing geochemical conditions. Appl. Environ. Microbiol. 79, 1171-1182.

648 Heinzel, E., Janneck, E., Glombitza, F., Schlömann, M., Seifert, J., 2009. Population
649 dynamics of iron-oxidizing communities in pilot plants for the treatment of acid mine
650 waters. Environ. Sci. Technol. 43, 6138-6144.

651 Huerta-Diaz, M.A., Tessier, A., Carignan, R., 1998. Geochemistry of trace metals
652 associated with reduced sulfur in freshwater sediments. Appl. Geochem. 13, 213-233.

653 Jacob, D.L., Otte, M.L., 2003. Conflicting processes in the wetland plant rhizosphere:
654 Metal retention or mobilization? Water Air Soil Pollut. Focus 3, 91-104.

655 Jameson, E., Rowe, O.F., Hallberg, K.B., Johnson, D.B., 2010. Sulfidogenesis and
656 selective precipitation of metals at low pH mediated by *Acidithiobacillus* spp. and
657 acidophilic sulfate-reducing bacteria. Hydrometallurgy 104, 488-493.

658 Johnson, D.B., Hallberg, K.B., 2005. Acid mine drainage remediation options: a review.
659 Sci. Total Environ. 338, 3-14.

660 Johnson, D.B., Hallberg, K.B., Hedrich, S., 2014. Uncovering a microbial enigma:
661 isolation and characterization of the streamer-generating, iron-oxidizing acidophilic
662 bacterium,"*Ferrovum myxofaciens*". Appl. Environ. Microbiol. 80, 672-680.

663 Kalbitz, K., Wennrich, R., 1998. Mobilization of heavy metals and arsenic in polluted
664 wetland soils and its dependence on dissolved organic matter. Sci. Total Environ. 209,
665 27-39.

666 Lai, W.-L., Zhang, Y., Chen, Z.-H., 2012. Radial oxygen loss, photosynthesis, and
667 nutrient removal of 35 wetland plants. Ecol. Eng. 39, 24-30.

668 Li, X., Rui, J., Xiong, J., Li, J., He, Z., Zhou, J., Yannarell, A.C., Mackie, R.I., 2014.
669 Functional potential of soil microbial communities in the maize rhizosphere. PLOS One
670 9, e112609.

671 Lin, C., Lu, W., Wu, Y., 2005. Agricultural soils irrigated with acidic mine water: acidity,
672 heavy metals, and crop contamination. Soil Research 43, 819-826.

673 Liu, F., Ni, H.-G., Chen, F., Luo, Z.-X., Shen, H., Liu, L., Wu, P., 2012. Metal
674 accumulation in the tissues of grass carps (*Ctenopharyngodon idellus*) from fresh water
675 around a copper mine in Southeast China. Environ. Monit. Assess. 184, 4289-4299.

676 Lüdemann, H., Arth, I., Liesack, W., 2000. Spatial changes in the bacterial community
677 structure along a vertical oxygen gradient in flooded paddy soil cores. Appl. Environ.
678 Microbiol. 66, 754.

679 Luther, G.W., Rickard, D.T., Theberge, S., Olroyd, A., 1996. Determination of metal
680 (bi)sulfide stability constants of Mn^{2+}, Fe^{2+}, Co^{2+}, Ni^{2+}, Cu^{2+}, and Zn^{2+} by voltammetric
681 methods. Environ. Sci. Technol. 30, 671-679.

682 Machel, H.G., 1989. Relationships between sulphate reduction and oxidation of organic
683 compounds to carbonate diagenesis, hydrocarbon accumulations, salt domes, and
684 metal sulphide deposits. Carbonate. Evaporite. 4, 137.

685 Machemer, S.D., Wildeman, T.R., 1992. Adsorption compared with sulfide precipitation
686 as metal removal processes from acid mine drainage in a constructed wetland. J.
687 Contam. Hydrol. 9, 115-131.

688 Marchand, L., Mench, M., Jacob, D.L., Otte, M.L., 2010. Metal and metalloid removal in
689 constructed wetlands, with emphasis on the importance of plants and standardized
690 measurements: A review. Environ. Pollut. 158, 3447-3461.

691 McKnight, D.M., Feder, G.L., 1984. The ecological effect of acid conditions and
692 precipitation of hydrous metal oxides in a Rocky Mountain stream. Hydrobiologia 119,
693 129-138.

694 Muyzer, G., Stams, A.J., 2008. The ecology and biotechnology of sulphate-reducing
695 bacteria. Nat. Rev. Microbiol. 6, 441-454.

696 Oueslati, W., van de Velde, S., Helali, M.A., Added, A., Aleya, L., Meysman, F.J.R.,
697 2019. Carbon, iron and sulphur cycling in the sediments of a Mediterranean lagoon
698 (Ghar El Melh, Tunisia). Estuar. Coast. Shelf Sci. 221, 156-169.

699 Petri, R., Podgorsek, L., Imhoff, J.F., 2001. Phylogeny and distribution of the sox B
700 gene among thiosulfate-oxidizing bacteria. FEMS Microbiol. Lett. 197, 171-178.

701 Ratering, S., Schnell, S., 2000. Localization of iron-reducing activity in paddy soilby
702 profile studies. Biogeochemistry 48, 341-365.

703 Rice, E.W., Baird, R.B., Eaton, A.D., Clesceri, L.S. (Eds.), 2012. Standard Methods for
704 the Examination of Water and Wastewater, 22nd edition. American Public Health
705 Association (APHA), American Water Works Association (AWWA) and Water
706 Environment Federation (WEF), Washington, D.C., USA.

707 Rodríguez-Germade, I., Rubio, B., Rey, D., 2014. XRF scanners as a quick screening
708 tool for detecting toxic pollutant elements in sediments from Marín harbour in the Ría
709 de Pontevedra (NW Spain). Mar. Pollut. Bull. 86, 458-467.

710 Rodríguez-Germade, I., Rubio, B., Rey, D., Borrego, J., 2015. Detection and
711 monitoring of REEs and related trace elements with an Itrax™ core scanner in the Ría
712 de Huelva (SW Spain). Water Air Soil Pollut. 226, 137.

713 Rothwell, R.G., Hoogakker, B., Thomson, J., Croudace, I.W., Frenz, M., 2006. Turbidite
714 emplacement on the southern Balearic Abyssal Plain (western Mediterranean Sea)

715 during Marine Isotope Stages 1–3: an application of ITRAX XRF scanning of sediment
716 cores to lithostratigraphic analysis. Geol. Soc. SP 267, 79-98.

717 Scheinost, A.C., 2005. Metal Oxides. In: Hillel, D. (Ed.). Encyclopedia of Soils in the
718 Environment. Elsevier, Oxford, pp. 428-438.

719 Scholz, M., Lee, B.h., 2005. Constructed wetlands: a review. Int. J. Environ. Stud. 62,
720 421-447.

721 Tjallingii, R., Röhl, U., Kölling, M., Bickert, T., 2007. Influence of the water content on
722 X-ray fluorescence core-scanning measurements in soft marine sediments. Geochem.
723 Geophy. Geosy. 8, Q02004.

724 Tribovillard, N., Algeo, T.J., Lyons, T., Riboulleau, A., 2006. Trace metals as
725 paleoredox and paleoproductivity proxies: An update. Chem. Geol. 232, 12-32.

726 Valkanas, M.M., Trun, N.J., 2018. A seasonal study of a passive abandoned coalmine
727 drainage remediation system reveals three distinct zones of contaminant levels and
728 microbial communities. MicrobiologyOpen, e00585.

729 von der Heyden, C.J., New, M.G., 2004. Sediment chemistry: a history of mine
730 contaminant remediation and an assessment of processes and pollution potential. J.
731 Geochem. Explor. 82, 35-57.

732 Vranken, M., Oenema, O., Mulder, J., 1990. Effects of tide range alterations on salt
733 marsh sediments in the Eastern Scheldt, S. W. Netherlands. Hydrobiologia 195, 13-20.

734 Yang, C., Lu, G., Chen, M., Xie, Y., Guo, C., Reinfelder, J., Yi, X., Wang, H., Dang, Z.,
735 2016. Spatial and temporal distributions of sulfur species in paddy soils affected by
736 acid mine drainage in Dabaoshan sulfide mining area, South China. Geoderma 281,
737 21-29.

738 Zhuang, P., McBride, M.B., Xia, H., Li, N., Li, Z., 2009. Health risk from heavy metals
739 via consumption of food crops in the vicinity of Dabaoshan mine, South China. Sci.
740 Total Environ. 407, 1551-1561.

741 Zwolsman, J.J.G., Berger, G.W., Van Eck, G.T.M., 1993. Sediment accumulation rates,
742 historical input, postdepositional mobility and retention of major elements and trace
743 metals in salt marsh sediments of the Scheldt estuary, SW Netherlands. Mar. Chem.
744 44, 73-94.

745

746

747

Figures

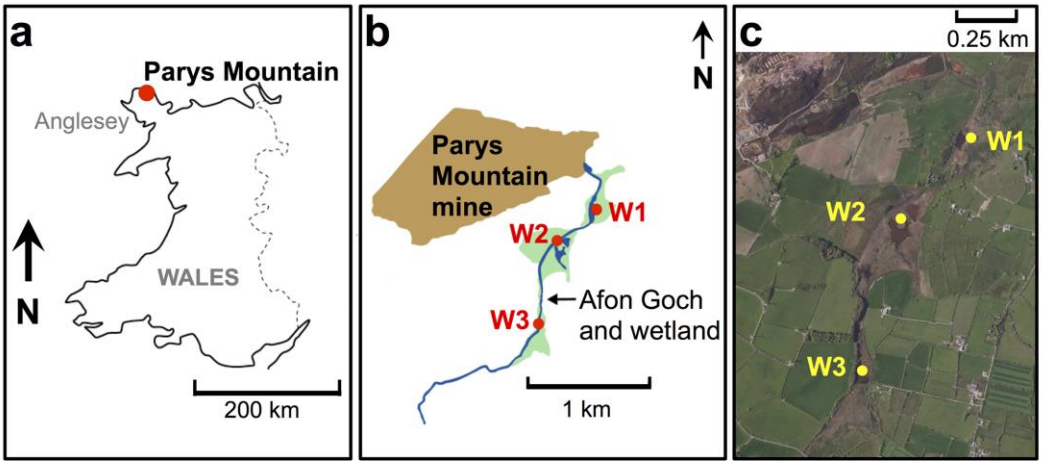

Figure 1. Location of sampling sites. (a) The Parys Mountain mine is located in Anglesey, Wales, UK. (b and c) Sites W1, W2 and W3 are along the Afon Goch river within a natural wetland.

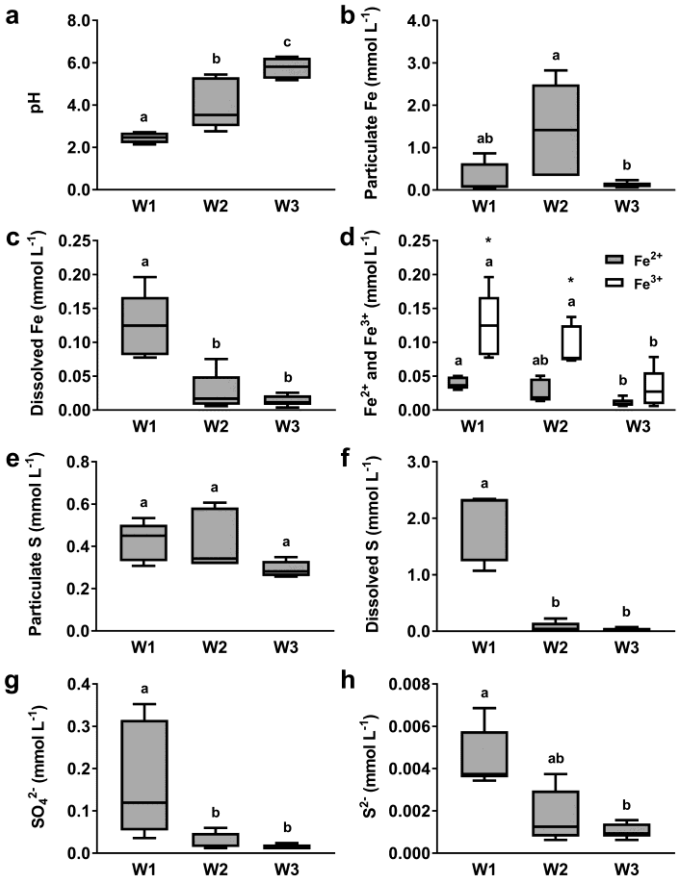

754

755 **Figure 2.** Fe, S and pH water chemistry parameters within the Afon Goch river as it
756 flows through the wetland. Mean values (n = 5) of pH (a), particulate Fe (b), dissolved
757 Fe (c), Fe^{2+} and Fe^{3+} (d), particulate S (e), dissolved S (f), sulfate (g) and sulfide (h).
758 For data in (a) error bars show standard deviation. For data in (b) – (h), boxes show the
759 25^{th} and 75^{th} percentile values, the black line within the boxes shows the median value,
760 and whisker bars show the minimum and maximum values. Values that do not share
761 lowercase letters are significantly different ($P < 0.05$). For data in (d) Fe^{3+} values with
762 an asterisk are significantly different ($P < 0.05$) from the Fe^{2+} values at that site.

763

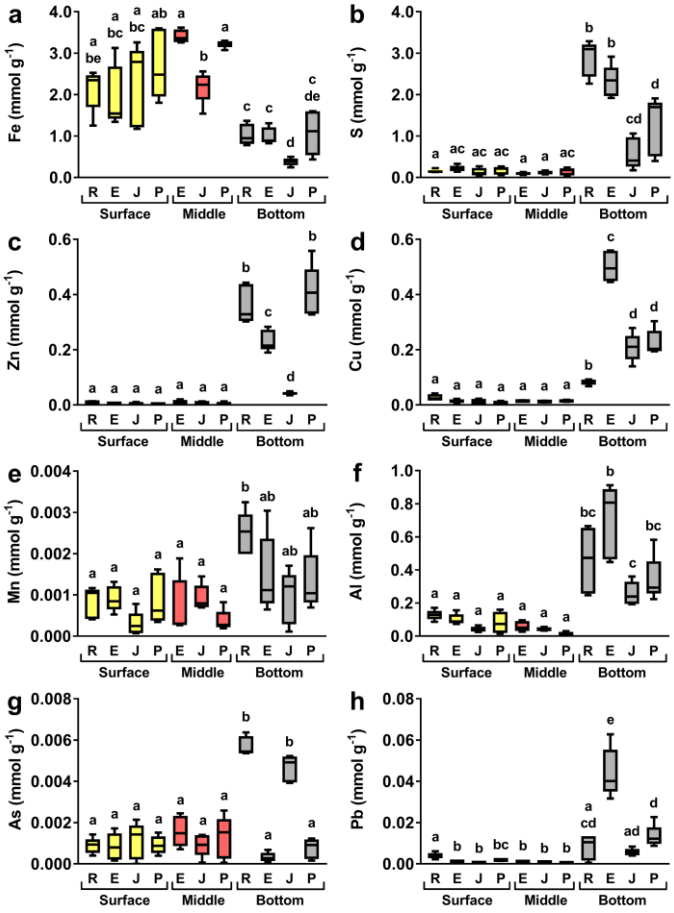

764

765 **Figure 3.** Mean values (n = 3) of total Fe (a), S (b), Cu (c), Zn (d), Mn (e), Al (f), As (g)
766 and Pb (h) in sediment bands from three depths (surface: 0 – 10 cm; middle: 10 – 20
767 cm; bottom: 20 – 50 cm) within the middle of the Afon Goch wetland (site W2). Cores
768 were taken at un-vegetated river (R) location, within the *E. angustifolium* (E) stand,
769 within the *Juncus* sp. (J) stand, and within the *P. australis* (P) stand. A distinct middle
770 band of sediment was absent within the river location cores. Boxes show the 25th and
771 75th percentile values, the black line within the boxes shows the median values, and
772 whisker bars show the minimum and maximum values. Values that do not share
773 lowercase letters are significantly different ($P < 0.05$).

774

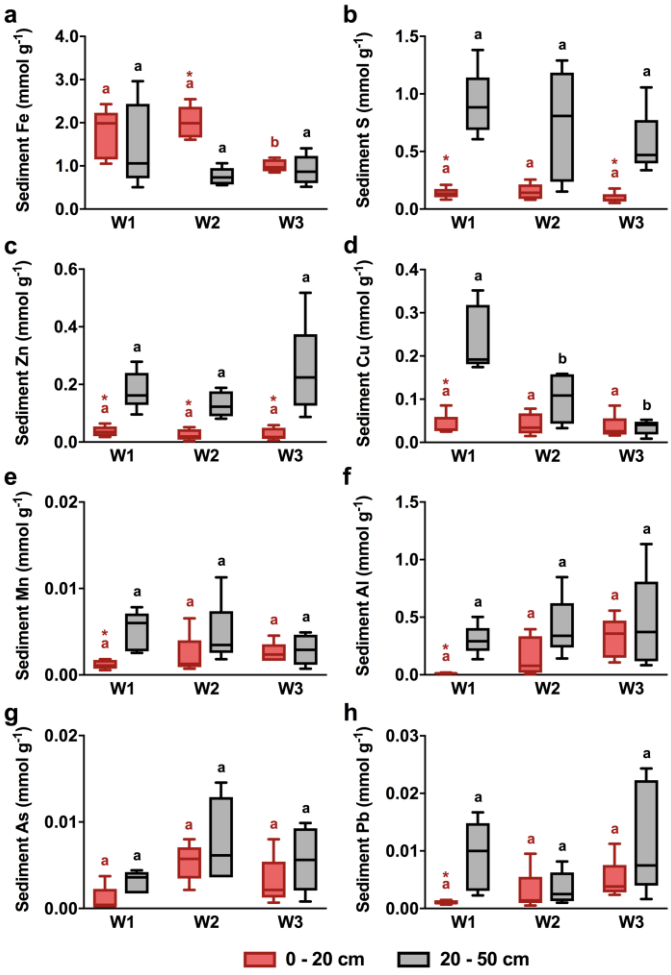

Figure 4. Mean values (n = 5) of Fe (a), S (b), Zn (c), Cu (d), Mn (e), Al (f), As (g), and Pb (h) in top (0 – 20 cm) and bottom (20 – 50 cm) sediment layers. Boxes show the 25th and 75th percentile values, the black line within the boxes shows the median values and whisker bars show the minimum and maximum values. Values within each sediment sample between sites that do not share lowercase letters are significantly different ($P < 0.05$). Values within the top sediment samples with an asterisk are significantly different ($P < 0.05$) from the bottom sediment sample values at that site.

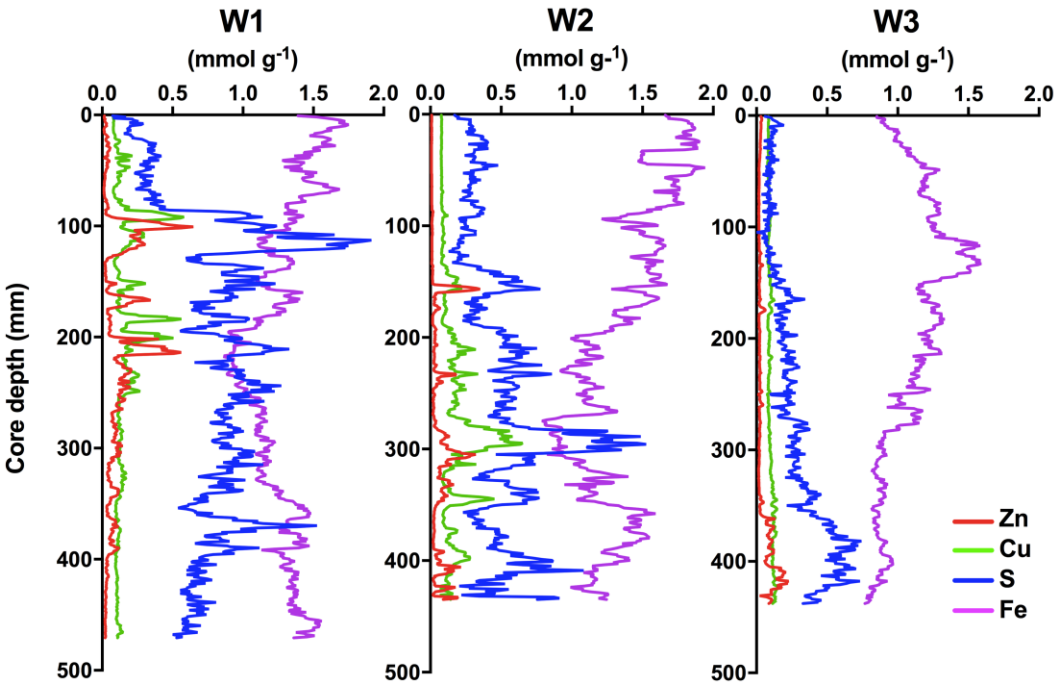

784

785 **Figure 5.** Profiles of Fe, S, Cu and Zn along sediment depths using X-ray fluorescence

786 scanning of cores from each site. Lines represent the mean of 3 replicate sediment

787 cores. Individual element profiles with error values are shown in Figure S4.

788

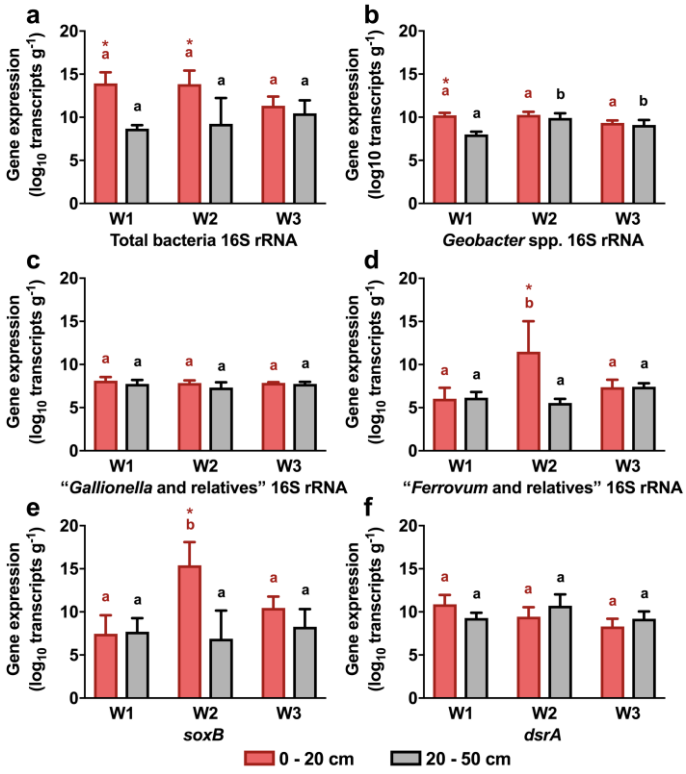

789

790 **Figure 6.** Mean values (n = 5) of 16S rRNA, *soxB* and *dsrA* transcript abundance from
791 RNA isolated from surface and bottom sediment layers from the Afon Goch wetland.
792 The different transcripts are markers for all bacteria (a), for Fe reducing bacteria of
793 *Geobacter* spp. (b), for Fe oxidizing bacteria of *Gallionella* and relatives spp. (c) and
794 *Ferrovum* and relatives spp. (d), and for S oxidizing bacteria through detection of *soxB*
795 (e) and S reducing bacteria through detection of *dsrA* (f). Error bars show the standard
796 deviation. Values within each sediment sample between sites that do not share
797 lowercase letters are significantly different ($P < 0.05$). Values within the top sediment
798 samples with an asterisk are significantly different ($P < 0.05$) from the bottom sediment
799 sample values at that site.

800

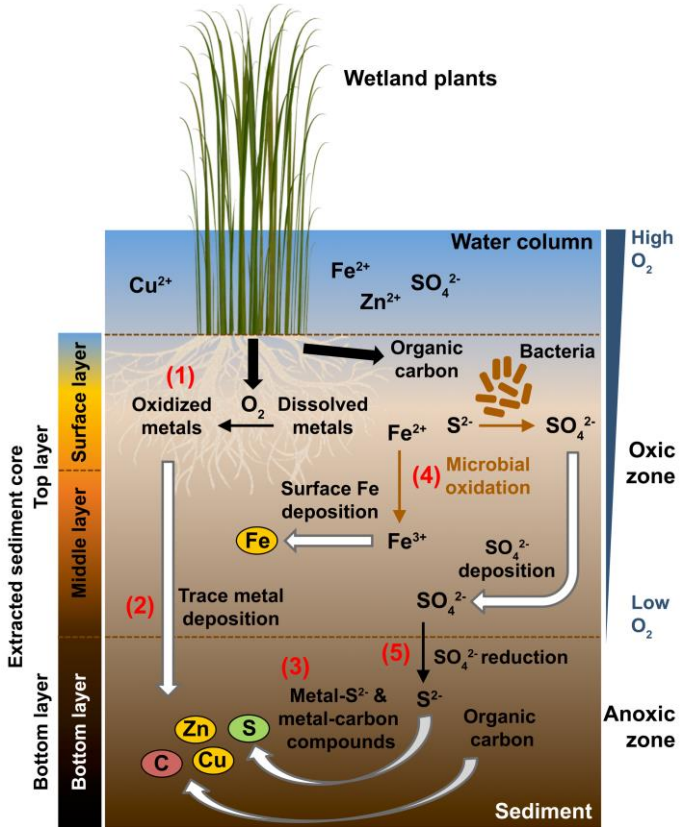

801

802 **Figure 7.** Model of wetland sediment metal deposition mediated by geochemical and
803 biochemical reactions. See the main text for the description of the key points (1 – 5). A
804 representation of the sediment cores indicating the three layers is shown; a surface
805 layer (~10 cm) that is partly aqueous and also contains larger soil particles and plant
806 roots; a middle layer (~10 cm) that is characterized by a red-brown color with
807 compacted ochre; and a bottom layer (~30 cm) that is composed of black anoxic mud.